Forced oscillation source localization from generator measurements

Melvyn Tyloo, ¹ Marc Vuffray² and Andrey Y. Lokhov²

Abstract—Malfunctioning equipment, erroneous operating conditions or periodic load variations can cause periodic disturbances that would persist over time, creating an undesirable transfer of energy across the system - an effect referred to as forced oscillations. Wide-area oscillations may damage assets, trigger inadvertent tripping or control actions, and be the cause of equipment failure. Unfortunately, for wide-area oscillations, the location, frequency, and amplitude of these forced oscillations may be hard to determine. Recently, a data-driven maximumlikelihood-based method was proposed to perform source localization in transmission grids under wide-area response scenarios. However, this method relies on full PMU coverage and all buses having inertia and damping. Here, we extend this method to realistic scenarios which includes buses without inertia or damping, such as passive loads and inverter-based generators. Incorporating Kron reduction directly into the maximum likelihood estimator, we are able to identify the location and frequency of forcing applied at both traditional generators and loads.

I. Introduction

Forced oscillations refer to periodic input signals that originate from malfunctioning devices in the power grid. Potential impacts of wide-area sustained oscillations include reduction of the effective transmission line capacities and, on the long run, damage to critical components in the grid [1], [2]. While most forced oscillations remain local and do not spread across the whole grid, threatening and difficult situations arise when forced oscillations are the causes of long-range disturbances. This happens when the input frequency is close to a natural mode of the system and triggers inter-area oscillations, as it was the case in the November 29, 2005 Western American Oscillation event across the Western Interconnection [2]. In such a scenario, the frequencies of wide areas of the grid swing against each other, inducing problems with automatic controllers and leading to possible line tripping. A wellknown wide-area forced oscillation event has been observed on January 11, 2019 in the Eastern Interconnection of the U.S. power grid, where significant frequency fluctuations were measured across thousands of kilometers within the system. The root cause was eventually found to be a malfunctioning steam turbine in Florida which has been disconnected only after 18 min [3]. Other major events of this type are

*This work has been supported by the Laboratory Directed Research and Development program of Los Alamos National Laboratory under project numbers 20220797PRD2, 20220774ER, and 20240734DI: Science fAIr Project, by U.S. DOE/SC Advanced Scientific Computing Research Program, and by U.S. DOE/OE Advanced Sensor and Data Analytics Program.

¹MT is with the Living Systems Institute, University of Exeter, Exeter, EX4 4QD, United Kingdom, the Department of Mathematics and Statistics, Faculty of Environment, Science, and Economy, University of Exeter, Exeter, EX4 4QD, United Kingdom, the Center for Nonlinear Studies (CNLS) and Theoretical Division, Los Alamos National Laboratory Los Alamos, NM, USA m.s.tyloo@exeter.ac.uk

²MV and AL are with the Theoretical Division, Los Alamos National Laboratory Los Alamos, NM, USA {vuffray,lokhov}@lanl.gov

surveyed in Ref. [4]. Due to their global effect on the grid, locating the source and identifying the frequency of wide-area forced oscillations represent a hard inference problem. Indeed, transmission power grids are typically made of thousands of components subject to an ever increasing complexity within the ongoing energy transition, and whose dynamic behavior is not always precisely known. More and more inverterbased resources - renewable energy sources connected to the grid through power electronics - penetrate the grid, which, together with the aging of existing components, make forced oscillations events more likely. It is therefore an important task to develop algorithms that are able to locate the source and identify the frequency of forced oscillations, so that they can be mitigated swiftly. Larger amount of real-time data is collected nowadays, thanks to the increasing number of Phasor Measurement Units (PMUs) on the grids, which opens the way to new data-driven algorithms [5]-[10].

Various methods have been proposed to identify forced oscillations: for instance, based on the complete knowledge of the grid dynamics [11], [12], specific grid topologies [13], knowledge of empirical wave propagation speed [14] or using local physical properties [15], [16], precise generator models [17], [18], specific structure in the data [19] or leveraging black-box machine learning methods [20]–[22].

Recently, Delabays et al. [23] proposed a promising location and identification method that does not require any prior knowledge about the grid dynamics or parameters, namely line capacities, inertia and primary control coefficients of the buses. This approach, that relies on a complete observation of the network behavior, is fully data-driven and is based on a maximum-likelihood estimator. However, while the deployment of PMUs has been constantly increasing over the past years, the full coverage of the grid is far from being achieved. Another restrictive assumption in [23] is that all buses have non-vanishing inertia and damping coefficients, which does not generically capture the behavior of loads or inverter-based resources. In this work we propose to address the shortcoming of [23]. More precisely, we improved the maximum-likelihood approach of Delabays et al. and develop an algorithm that accommodates for buses with lack of inertia and damping and that accounts for partial PMU coverage of the transmission network. We consider a more realistic setting for which major system components such as generator buses are typically observed, whereas measurements at other buses with no inertia and damping such as loads and inverter-based resources are generally not available. We also assume that we know the grid topology and line susceptances but that we do not have access to other system parameters such as inertia, damping of the generators and/or load consumption and inverter generation. In order to allow for a prompt localization and identification of the source of forced oscillations, we assume that the

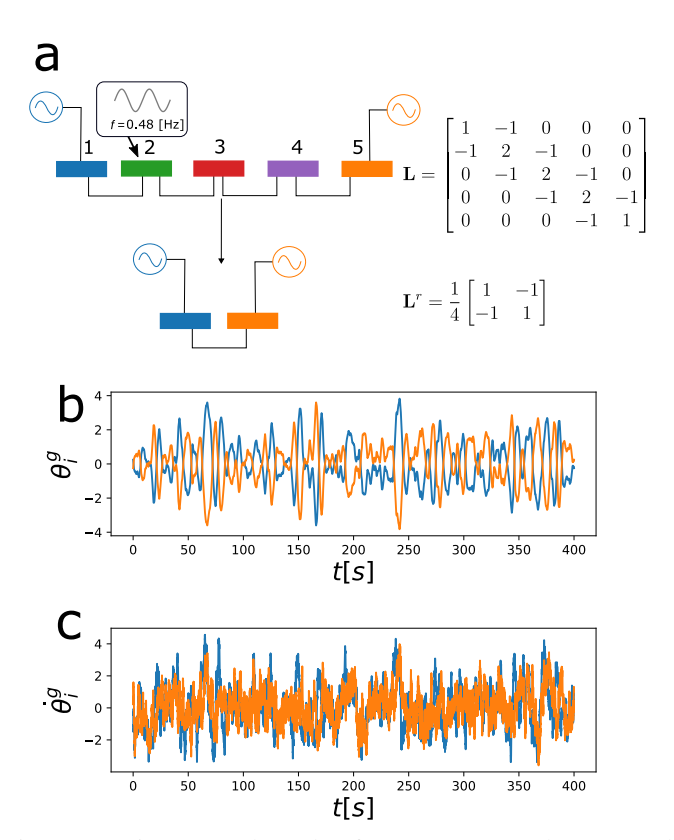


Fig. 1: (a) Line network made of two generators (buses 1 and 5) and three load/inverter-based resource buses (2, 3, 4) with its corresponding Laplacian matrix L. After the Kron reduction, the system reduces to two generators with a new effective coupling Laplacian matrix L^r . The matrix entries are given by the transmission line susceptances. (b), (c) Time-series of the angle (b) and frequency (in [rad/s]) (c) deviations at the two generators with corresponding colors when a forcing with frequency of 0.48Hz is applied at the load bus 2 [in green in panel (a)]. They are obtained by simulating the reduced grid model Eq. (8). Note that on the angle time-series, we have subtracted their average value at each time step. The forcing amplitude is $\gamma = 1$ which is similar to the noise strength. The colors correspond to those of panel (a). Generators have inertia and damping parameters, $d_1 = 0.3s$, $d_2 = 1s$, $m_1 = 1.4s^2$, $m_2 = 1.1s^2$.

observation time frame is relatively short and on the order of hundreds of seconds. On this time-scale, the fluctuations in the grid dynamic can be considered to obey the swing dynamic equations to a good approximation [6]. Our approach is based on an explicit Kron reduction of the dynamics [24], [25] that can be directly incorporated into the objective function expressing the likelihood of observations at the generators. We show that this formulation, combined with a preliminary identification of the inertia and damping parameters, allows us to successfully locate the source and identify the frequency of the forcing both when it is applied at generators or at unobserved load/inverter-based resource buses.

The contributions can be summarized as follows:

 We develop a likelihood approach for the detection and localization of forced oscillations in realistic high-voltage grids.

- We consider a grid model where not all buses are generators, but instead can be either generators or inverter based resources/load buses.
- Not only we adapt and extend the method of Ref. [23] to a
 more realistic grid model, but we also go beyond the full
 observability assumption and instead suppose that only
 PMU measurement time-series at the generator buses are
 accessible.

The paper is organized as follows. We start by defining the notations in Sec. II. Then, in Sec. III, we introduce the dynamical model and its Kron reduction. Section IV presents the localization and identification algorithm. We illustrate the algorithm on a toy example in Sec. V and the IEEE-57 bus test case in Sec. VI. A comparison with existing methods is done in Sec. VII. In Sec. VIII, we apply the localization algorithm to realistic PMU time-series. The conclusions are given in Sec. VI.

II. NOTATIONS

In the following, we denote column vectors $\mathbf{v} \in \mathbb{R}^N$ as bold lowercase letters and their transpose vectors as \mathbf{v}^\top . Matrices $\mathbf{A} \in \mathbb{R}^{N \times N}$ are referred to with bold uppercase letters. The l-th canonical basis vector is denoted \mathbf{e}_l . The expectation value of a random variable ξ is denoted $\langle \xi \rangle$. We denote the components of the identity matrix \mathbf{I} using the Kronecker delta δ_{ij} .

III. SWING DYNAMICS AND FORCED OSCILLATIONS

We consider high-voltage power transmission networks that are composed of generator (\mathcal{G}) and load/inverter-based resource (\mathcal{L}) buses. At each bus, one has a complex-valued voltage variable whose phase and frequency at bus i is denoted Θ_i and $\dot{\Theta}_i$, respectively. In the lossless line approximation, the dynamics of the phase of the voltage at each bus is described by the swing equations [26]:

$$m_i \ddot{\Theta}_i + d_i \dot{\Theta}_i = P_i - \sum_j B_{ij} (\Theta_i - \Theta_j) + \eta_i^g, i \in \mathcal{G} \quad (1)$$
$$0 = P_i - \sum_j B_{ij} (\Theta_i - \Theta_j) + \eta_i^l, i \in \mathcal{L}, \quad (2)$$

where the inertia and damping coefficients are denoted m_i and d_i , and P_i is the generated $(P_i>0)$ or consumed $(P_i<0)$ power. The line susceptances b_{ij} are included in the coupling as $B_{ij}=|V_i||V_j|b_{ij}$, where we assume the voltage amplitudes $|V_i|$'s to be constant over time. Consumption fluctuations around the nominal operation set-point are modelled by i.i.d. Gaussian variables $\eta_i^{g,l}$. In the above model, the generator response is described on these time scale by the (linear) swing equations, while loads with no inertia and damping instantaneously adapt to the power fluctuations. Such dynamics could also described grid-following inverter-based resources whose control algorithms are much faster than the grid dynamics. The forced oscillations coming from a faulty component at node l is modeled by an additive term $\gamma \cos(2\pi(ft+\phi))$ with amplitude γ , frequency f, and phase ϕ , acting at a single generator or load bus. Since loads with no inertia and damping

are described by a much faster dynamics, here modeled by an instantaneous response in Eq. (2), we can work on a restrained dynamical model which relate model parameters to observations at the generators with the help of a Kron reduction, derived as follows. We denote the Laplacian matrix of the grid,

$$L_{ij} = \begin{cases} -B_{ij} & i \neq j \\ \sum_{k} B_{ik} & i = j \end{cases}$$
 (3)

which is divided into four block according to generators and loads/inverter-based resources as,

$$\mathbf{L} = \begin{bmatrix} \mathbf{L}^{gg} & \mathbf{L}^{gl} \\ \mathbf{L}^{lg} & \mathbf{L}^{ll} \end{bmatrix} . \tag{4}$$

The Kron reduction of the network yields the smaller Laplacian matrix [24], [25],

$$\mathbf{L}^r = \mathbf{L}^{gg} - \mathbf{L}^{gl} (\mathbf{L}^{ll})^{-1} \mathbf{L}^{lg} \,. \tag{5}$$

When applying the reduction, one must also carefully modify the source term in Eqs. (1). The noise in the reduced network becomes,

$$\boldsymbol{\eta}^{gl} = \boldsymbol{\eta}^g - \mathbf{L}^{gl} (\mathbf{L}^{ll})^{-1} \boldsymbol{\eta}^l \,. \tag{6}$$

Since the power fluctuations are i.i.d., i.e. $\langle \eta_i^{g,l}(t) \eta_j^{g,l}(t) \rangle = \delta_{ij}$, then the variance of the effective noise is,

$$\langle \eta_i^{gl}(t)\eta_i^{gl}(t)\rangle = (\delta_{ij} + [\mathbf{L}^{gl}(\mathbf{L}^{ll})^{-2}\mathbf{L}^{lg}]_{ij}). \tag{7}$$

Including the forcing term and using a matrix notation, the equivalent dynamics observed at the generators takes the following form,

$$\begin{bmatrix} \dot{\boldsymbol{\theta}}^{g} \\ \ddot{\boldsymbol{\theta}}^{g} \end{bmatrix} = \begin{bmatrix} 0 & \mathbf{I} \\ -\mathbf{M}^{-1}\mathbf{L}^{r} & -\mathbf{M}^{-1}\mathbf{D} \end{bmatrix} \begin{bmatrix} \boldsymbol{\theta}^{g} \\ \dot{\boldsymbol{\theta}}^{g} \end{bmatrix} + \begin{bmatrix} 0 \\ \mathbf{M}^{-1}\boldsymbol{\eta}^{gl} \end{bmatrix} + \begin{bmatrix} 0 \\ \mathbf{M}^{-1}\mathbf{u} \end{bmatrix}$$
(8)

where $\theta^g = \Theta^g - \Theta^g_0$ are the deviations of the phases from the operational state Θ_0^g at the generator buses, M and D are the diagonal matrices of inertia and damping parameters whose diagonal elements are given by m_i and d_i , respectively. Similarly to the noise, the reduced power vector reads, \mathbf{P}^{gl} = $-\mathbf{L}^{gl}(\mathbf{L}^{ll})^{-1}\mathbf{P}$. The last term in Eq. (8) is the forcing which has different form depending on its location. If the forcing is applied to a generator bus, then $\mathbf{u} = \gamma \mathbf{e}_l \cos(2\pi (ft + \phi))$ with $l \in \mathcal{G}$, while if it is at a load/inverter-based resource, then $\mathbf{u} = -\gamma \mathbf{L}^{gl} \mathbf{L}^{ll^{-1}} \mathbf{e}_l \cos(2\pi (ft + \phi))$ with $l \in \mathcal{L}$, similar to Eq. (6). Therefore, in the Kron reduced dynamics, the forcing applied at $l \in \mathcal{L}$ potentially translates into multiple effective forcing sources applied to the neighboring generator buses. Let us illustrate this effect on a simple line grid with homogeneous susceptance shown in Fig. 1(a), where two generator buses (in blue and orange) are at the ends of the line grid, connected by three loads (in green, red and purple). In this case where the input is at bus 2, the effective forcing in the Kron reduced system reads as,

$$\mathbf{u}(t) = \frac{\gamma}{4} \begin{bmatrix} 3 & 2 & 1\\ 1 & 2 & 3 \end{bmatrix} \mathbf{e}_l \cos(2\pi (ft + \phi)). \tag{9}$$

Quite intuitively, we observe that choosing the bus in the center of the grid in Fig. 1(a) as a source translates into two effective forcing inputs with same amplitude at the generators. Placing the forcing at one the two other loads also results in two effective forcing inputs at the generators, however, with amplitudes that are different: the one at the closest generator being larger than the other. Importantly, the same effective forcing can be obtained if one allows multiple sources of forcing at load/inverter-based resource buses. Indeed, for example having a single source at bus 2 of $\gamma = 1$ produces the same effect seen at the generators as having two sources: one at bus 3 with $\gamma = 2$ and one at bus 4 with $\gamma = 1$, and the opposite phase leading to an opposite-sign input. The multiplicity of the settings leading to the same observations at the generator buses makes the identification of the disturbance a very challenging problem. In the following, we assume that there is a single source of forced oscillations, and identify its parameters using measurements at the generator buses only.

The forced oscillation localization problem is formulated as follows: given measurements of the voltage phases and frequencies collected at the generators before and during the event (see Fig. 1(b) as an example), reconstruct the location, amplitude, and frequency of the forced oscillation which may originate from any bus in the grid. As mentioned earlier, we assume that the grid topology and line susceptances are known. However, we do not assume that neither the damping and inertia coefficients associated with the generators, nor the frequency, phase, and location parameters associated with the forcing are available. Hence, we aim at performing a sequential identification of both the unknown system and the forcing parameters. We do assume that the noise is homogeneous at all buses.

IV. LOCALIZATION AND IDENTIFICATION METHOD

In the previous section, we showed that the load/inverter-based resource buses can be eliminated, producing an effective dynamics observed at the generators. Due to this elimination, the effective forcing originating from the load buses can be very similar and even identical, depending on the coupling topology of the grid. To tackle the challenge of correctly identifying the source of forced oscillations even at load buses, we propose a two-step approach. First, we learn the dynamical parameters, namely \mathbf{M} , \mathbf{D} , using a method of moments and the knowledge of the grid topology while observing the grid subject to ambient noise. Second, assuming that the grid is subject to a forced oscillation event, we use the estimates for \mathbf{M} , \mathbf{D} to define a log-likelihood cost function of the location, frequency and phase of the source based on the observed time-series at the generators, following the ideas proposed in [23].

A. Step 1: Estimation of the dynamical parameters

To obtain an estimate of M, D, knowing the L^r , we use a maximum likelihood approach [7]. The latter essentially rely on the fluctuations of the system around its operational state. We consider a time-discretized version of the effective continuous stochastic dynamics at the generators, assuming that we have computed the reduced Laplacian matrix L^r . Denoting

the measurements of the deviation from the operational state at the generators at time t_i and the dynamics matrix,

$$\mathbf{X}_{t_i} = \begin{bmatrix} \boldsymbol{\theta}_{t_i}^g \\ \dot{\boldsymbol{\theta}}_{t_i}^g \end{bmatrix} , \mathbf{A} = \begin{bmatrix} 0 & \mathbf{I} \\ -\mathbf{M}^{-1}\mathbf{L}^r & -\mathbf{M}^{-1}\mathbf{D} \end{bmatrix} , \quad (10)$$

respectively, and using a Euler-Maruyama approximation scheme of Eq. (8), we can reformulate the dynamics when there is no forcing as the first-order system with discretized time steps ordered with i = 1, ..., N - 1,

$$\boldsymbol{\Delta}_{t_i} = \mathbf{A} \mathbf{X}_{t_i} + \begin{bmatrix} \mathbf{0} & \mathbf{M}^{-1} \boldsymbol{\eta}^{gl} \end{bmatrix}^{\top}, \tag{11}$$

where $\Delta_{t_i} = (\mathbf{X}_{t_{i+1}} - \mathbf{X}_{t_i})/ au$ with time-step au = T/N and Tthe length of the time-series such that $t_i = i\tau$. Multiplying the later equation by $\mathbf{X}_{t_i}^{ op}$ on the right and taking the expectation yields,

$$\mathbf{S}_1 = \mathbf{A} \, \mathbf{S}_0 \tag{12}$$

where we defined $\mathbf{S}_1 = \mathbb{E}[\mathbf{\Delta}_{t_i}\mathbf{X}_{t_i}^{\top}], \, \mathbf{S}_0 = \mathbb{E}[\mathbf{X}_{t_i}\mathbf{X}_{t_i}^{\top}]$. One therefore has the estimate $\hat{\mathbf{A}} = \mathbf{S}_1 \mathbf{S}_0^{-1}$ from which, thanks to the knowledge of the grid topology, one can extract estimates for the inertia and damping parameters $\hat{\mathbf{M}}$, $\hat{\mathbf{D}}$.

B. Step 2: Localization of the source

In order to write down the likelihood estimators of these parameters, we consider the time-discretized version of the dynamics given in the previous subsection, where we add on the right-hand side of Eq. (11) the forcing term $\begin{bmatrix} \mathbf{0} & \mathbf{M}^{-1}\mathbf{u}(k) \end{bmatrix}$ where we defined,

$$\mathbf{u}(k) = \begin{cases} \gamma \, \mathbf{e}_{l} \operatorname{Re} \left(e^{2\pi j (k \frac{i}{N} + \phi)} \right), l \in \mathcal{G} \\ -\gamma \, \mathbf{L}^{gl} \mathbf{L}^{ll^{-1}} \mathbf{e}_{l} \operatorname{Re} \left(e^{2\pi j (k \frac{i}{N} + \phi)} \right), l \in \mathcal{L} \end{cases}$$
(13)

and the frequency of the forcing that relates to the integer 0 < k < N/2 with k = fT. Using this discretization, we define log-likelihood function to identify the frequency and localize the source of the forcing as,

$$\tilde{L}(\gamma, l, k, \phi \mid \{X_{t_i}\}_{i=1}^{N}, \mathbf{L}^r, \hat{\mathbf{M}}, \hat{\mathbf{D}})$$

$$= \frac{1}{N} \sum_{i=0}^{N-1} \mathbf{v}_{t_i}^{\mathsf{T}} \mathbf{\Sigma}_{gl}^{-1} \mathbf{v}_{t_i}, \tag{14}$$

with

$$\mathbf{v}_{t_i} = \hat{\mathbf{M}} \left[\mathbf{\Delta}_{t_i} - \mathbf{A} \mathbf{X}_{t_i} \right]_2 - \mathbf{u}(k) , \qquad (15)$$

$$\mathbf{\Sigma}_{al}^{-1} = \left(\left[\mathbf{I} + \mathbf{L}^{gl} (\mathbf{L}^{ll})^{-2} \mathbf{L}^{lg} \right] \right)^{-1} , \qquad (16)$$

$$\mathbf{\Sigma}_{gl}^{-1} = ([\mathbf{I} + \mathbf{L}^{gl}(\mathbf{L}^{ll})^{-2}\mathbf{L}^{lg}])^{-1}, \qquad (16)$$

where the index 2 in Eq. (15) refers to the second half of the vector. More precisely, Eq. (14) is the normalized log-likelihood for the unknown parameters (γ, l, k, ϕ) given $(\{X_{t_j}\}_{j=1}^N, \mathbf{L}^r, \hat{\mathbf{M}}, \hat{\mathbf{D}})$. The objective function in Eq. (14) is essentially a least-squares estimator generalized to the case of a non-diagonal noise covariance matrix Σ resulting from the Kron reduction over the nodes \mathcal{L} . It is important to note the discrete set of forcing frequencies, which results from the finiteness of the time-series measurements i.e. T, and of the time-step τ , is essential in order to perform the optimization on Eq. (14). Indeed, keeping a continuous forcing frequency makes the optimization a much harder nonlinear problem to solve, as previously noted in [23] for a simpler version of the estimator. Even when both the frequency k and the location lof the forcing are fixed, the minimization over (γ, ϕ) is still a complex optimization problem. However, expanding the term inside the sum in Eq. (14), one notices that, using the discrete Fourier transform of the time-series,

$$\widetilde{\mathbf{X}}(k) = \frac{1}{\sqrt{N}} \sum_{i=0}^{N-1} e^{2\pi j \frac{k}{N} i} \mathbf{X}_{t_i} , \qquad (17)$$

$$\widetilde{\Delta}(k) = \frac{1}{\sqrt{N}} \sum_{i=0}^{N-1} e^{2\pi j \frac{k}{N} i} \Delta_{t_i},$$
(18)

there is effectively only a single term that depends on the phase ϕ independently of the other variables. Therefore, the optimization over ϕ can be performed explicitly, resulting in an easier problem. Overall an equivalent log-likelihood function over the remaining parameters is written as (see App. A for some details),

$$L\left(\gamma, l, k \mid \{\mathbf{X}_{t_i}\}_{i=0}^{N-1}, \mathbf{L}^r, \hat{\mathbf{M}}, \hat{\mathbf{D}}\right) = \frac{\gamma^2}{2} \alpha_1 - \gamma \alpha_2, \quad (19)$$

where we further defined.

$$\alpha_1 = \mathbf{\Gamma}_l^{\top} \mathbf{\Sigma}_{gl}^{-1} \mathbf{\Gamma}_l \,, \tag{20}$$

$$\alpha_2 = \frac{2}{\sqrt{N}} \left[\text{Tr} \left(\mathbf{G}_{22} \hat{\mathbf{D}} \mathbf{C} \hat{\mathbf{D}} \right) + 2 \text{Tr} \left(\mathbf{G}_{12} \hat{\mathbf{D}} \mathbf{C} \mathbf{L}^r \right) \right]$$

+Tr
$$\left(\mathbf{H}_{21}\hat{\mathbf{D}}\mathbf{C}\hat{\mathbf{D}}\right)$$
 + 2Tr $\left(\mathbf{G}_{11}\mathbf{L}^{r}\mathbf{C}\mathbf{L}^{r}\right)$ (21)

+
$$2\operatorname{Tr}\left(\mathbf{E}_{21}\mathbf{L}^{r}\mathbf{C}\hat{\mathbf{M}}\right)$$
 + $\operatorname{Tr}\left(\mathbf{H}_{22}\hat{\mathbf{M}}\mathbf{C}\hat{\mathbf{M}}\right)\right]^{1/2}$ (22)

$$\mathbf{C} = \mathbf{\Sigma}_{gl}^{-1} \mathbf{\Gamma}_{l} \mathbf{\Gamma}_{l}^{\top} \mathbf{\Sigma}_{gl}^{-1}, \ \mathbf{E}(k) = \operatorname{Re}[\tilde{\mathbf{\Delta}} \tilde{\mathbf{X}}^{\dagger}]$$
 (23)

$$\mathbf{G}(k) = \operatorname{Re}\left(\tilde{\mathbf{X}}\tilde{\mathbf{X}}^{\dagger}\right), \ \mathbf{H}(k) = \operatorname{Re}\left(\tilde{\boldsymbol{\Delta}}\tilde{\boldsymbol{\Delta}}^{\dagger}\right)$$
 (24)

$$\mathbf{\Gamma}_{l} = \begin{cases} \mathbf{e}_{l}, l \in \mathcal{G} \\ -\mathbf{L}^{gl} \mathbf{L}^{ll-1} \mathbf{e}_{l}, l \in \mathcal{L} \end{cases}$$
 (25)

with the lower indices referring to the four blocks of the matrices. The optimization of Eq. (19) over (γ, l, k) remains a non-convex problem. However, fixing both the location and the frequency, one can analytically find the optimal γ^* for each pair (l, k) in Eq. (19), which is given by,

$$\gamma^*(l, k \mid \{\mathbf{X}_{t_i}\}_{i=0}^{N-1}, \mathbf{L}^r, \hat{\mathbf{M}}, \hat{\mathbf{D}}) = \frac{\alpha_2}{\alpha_1}.$$
 (26)

The latter can then be substituted into Eq. (19) to obtain the log-likelihood.

The overall workflow of the method is illustrated in the chart given in Fig. 2. If, on top of the forced oscillation, one is aware of changes in the topology of the grid, such as a line that has tripped, this information can be included in the prior knowledge when performing step 2. One also remarks that, due to the Kron reduction, the matrix \mathbf{L}^r is not sparse anymore, which might affect the computational complexity of the matrix products in Eq. (19). In practice, this is counterbalanced by the fact that our method only requires access to measurements at a fraction of the buses, e.g. only 7 over the 57 buses in the IEEE-57 bus test case presented in Sec. VI.

Fig. 2: Diagram of the two steps (Secs. IV-A, IV-B) involved in the localization of the forced oscillations.

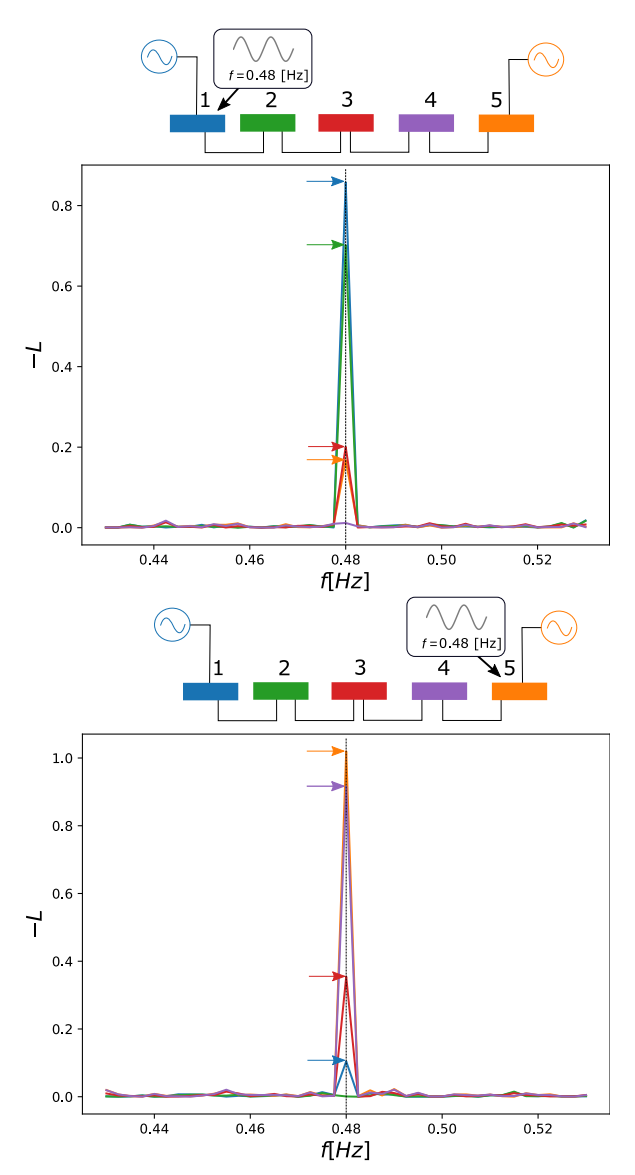


Fig. 3: Detection and localization of forced oscillations when the source is at a generator. The inertia and damping parameters are first learned on the system without forcing for 15min with measurements at 50Hz. The forcing with frequency 0.48Hz is applied at the leftmost (top panel) and rightmost (bottom panel) generator. The correct source and frequency are identified by the largest log-likelihood. The dashed vertical lines give the frequency 0.48Hz. The amplitude of the forcing is $\gamma=2$, and the time-series correspond to measurements at 50Hz over 400s. Generators have inertia and damping parameters, $d_1=1s$, $d_2=1s$, $m_1=1s^2$, $m_2=1s^2$.

In the following sections, we illustrate the performance of the method on synthetic test cases.

Note that, in the following sections, the time-series were simulated with a noise standard deviation set to unity, which is smaller than the forcing amplitude but still comparable in order of magnitude. We argue that this represents relevant operational conditions within forced oscillation events. Indeed, if the forcing strength is smaller than the noise amplitude, the forced oscillation event might not be a concern to the grid operator due to its barely observable effect.

V. TOY MODEL

We first consider a simple grid made of two generators and three loads/inverter-based resources as shown in Fig. 1(a). After performing the Kron reduction only the two generators remain with a coupling between them given by \mathbf{L}^r . We assume that the inertia and damping parameters are learned on the system without forcing during 15min with measurements at 50Hz only available at generator buses. Then, we perform the localization step on the system with forcing with measurements of length 400s also sampled at 50Hz and only available at generator buses. We first illustrate the algorithm in the simpler situation where the forcing is applied at one of the generators. Figure 3 shows the log-likelihood obtained from the optimization of Eq. (19) in this scenario, when a forcing with a frequency of 0.48Hz is applied at the generators. One observes that in both cases, the source and frequency of the forcing are correctly identified. Note that some other peaks are observed. These correspond to scenarios where multiple sources of forced oscillation occur at the same time. As the cost function L represents the log-likelihood divided by N, the likelihood of these other scenarios are exponentially suppressed as the number of samples N grows, which guarantees that for a sufficiently long time-series the source can be correctly identified. Generators inertia and damping parameters are given in the caption of Fig. 4.

We now move to a more challenging problem of source identification when the forcing is applied at a load/inverter-based resource bus. Figure 4 shows the outcome of the algorithm when a forcing of $0.48 \mathrm{Hz}$ is sequentially applied to each of the load/inverter-based resource bus. In every situation, the algorithm is able to correctly identify the source bus and the forcing frequency. Note the symmetry between the left and right panels which is due to the form of the forcing that are respectively given by,

$$\mathbf{\Gamma}_2 = -\frac{1}{4} \begin{bmatrix} 0 & 0 & 3 & 1 \end{bmatrix}^\top, \mathbf{\Gamma}_4 = -\frac{1}{4} \begin{bmatrix} 0 & 0 & 1 & 3 \end{bmatrix}^\top.$$
(27)

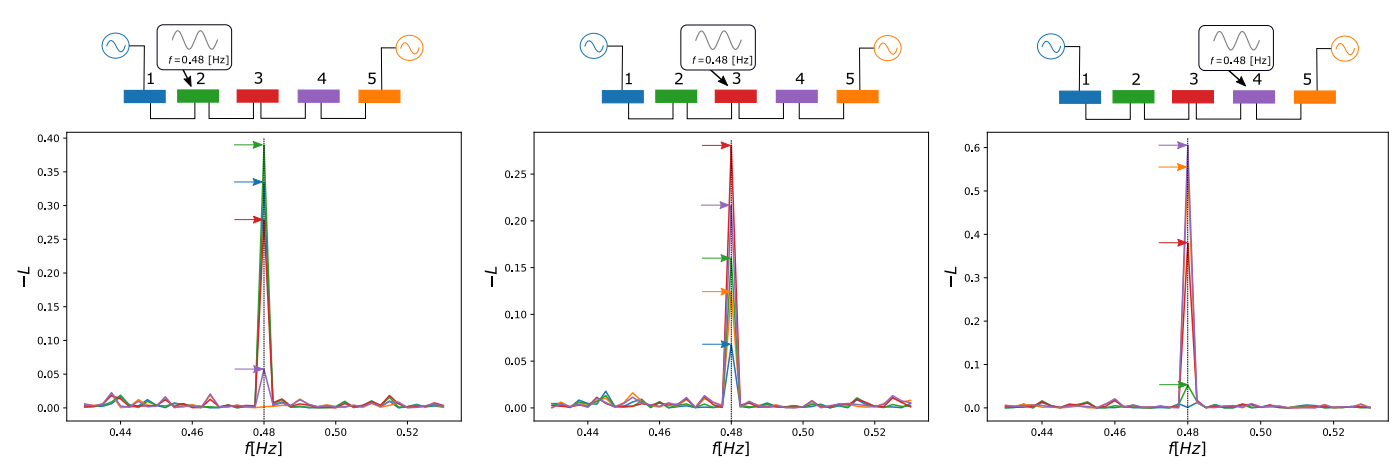


Fig. 4: Detection and localization of forced oscillations when the source is at a load/inverter-based resource bus. The inertia and damping parameters are first learned on the system without forcing for 15min with measurements at 50Hz. In all three cases when the forcing of 0.48Hz, which is close to a natural frequency of the system (see Fig. 1) is applied at bus 2 (left panel), 3 (middle panel), 4 (right panel), the correct source and frequency are identified by the largest log-likelihood. The dashed vertical lines give the frequency 0.48Hz. The amplitude of the forcing is $\gamma=2$, and the time-series correspond to measurements at 50Hz over 400s. Generators have inertia and damping parameters, $d_1=1s$, $d_2=1s$, $m_1=1s^2$, $m_2=1s^2$. The noise amplitude is set to unity.

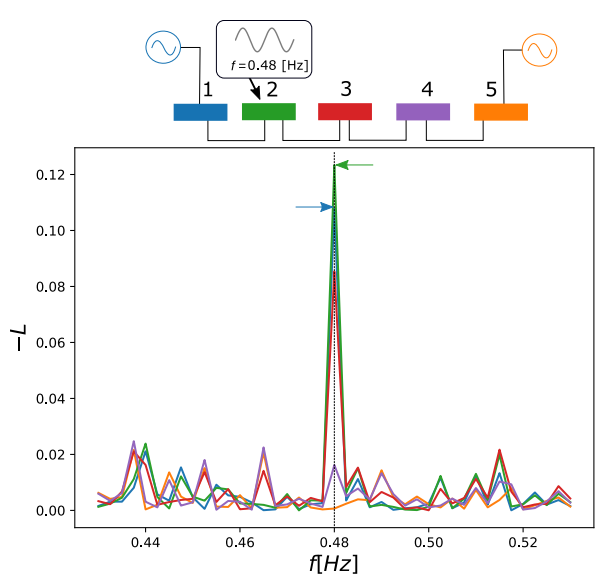


Fig. 5: Detection and localization of forced oscillations when the source is at a load/inverter-based resource bus. The inertia and damping parameters are first learned on the system without forcing for 15min with measurements at 50Hz. The amplitude of the forcing is $\gamma=1$, and the time-series correspond to measurements at 50Hz over 400s. Generators have inertia and damping parameters, $d_1=0.3s\,,\ d_2=1s\,,\ m_1=1.4s^2\,,\ m_2=1.1s^2\,.$

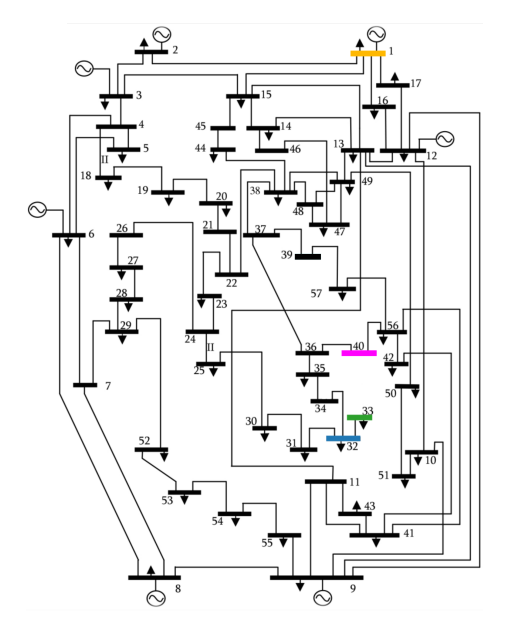


Fig. 6: Topology of the IEEE-57 bus test case, where the generators are located at the periphery of the grid. The blue and green load buses produce the same response (up to 10 decimals) at the generators when the forcing is applied at either of them. The line capacities are heterogeneous [27].

The slight discrepancy in the symmetry between the left and right panels is due to the different sequences of random variables used for the simulations and the finite sample size. This toy model already illustrates that even when the number of reduced buses is larger than the remaining number of generators, the algorithm is able to locate the source in the original grid. To push the algorithm to its limits, we finally

consider a challenging example where the amplitude of the forcing is comparable to the noise amplitude, and the inertia and damping parameters are heterogeneous. The outcome of the method is given in Fig. 5 where the correct load bus is identified together with the forcing frequency. To further demonstrate the performance of our method, in the next section we consider the IEEE-57 bus test case.

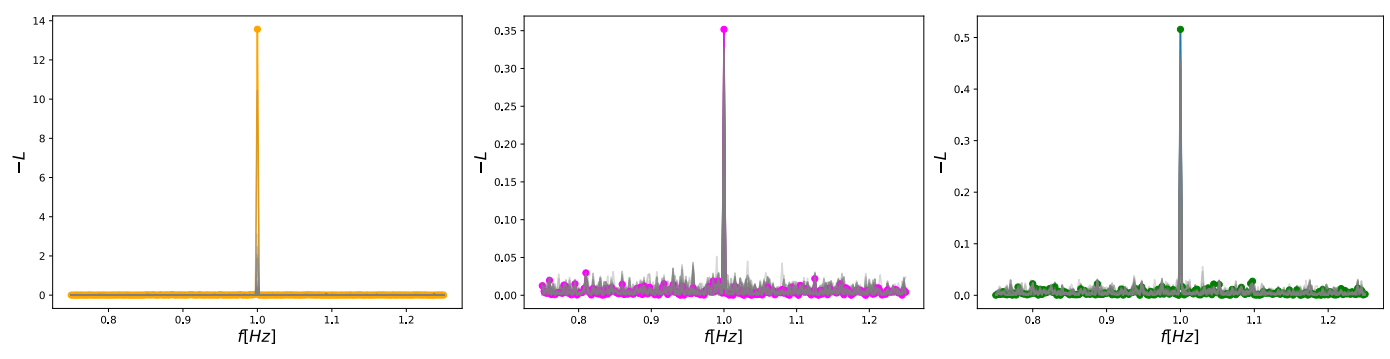


Fig. 7: Detection and localization of forced oscillations when the source is at the generator bus shown in orange (left panel), at the load bus in pink (center panel), and the load bus in green (right panel) in Fig 6. In the latter case, both sources are indistinguishable from each other, i.e., both buses have the same likelihood as $\Gamma_{32} \cong \Gamma_{33}$. The forcing frequency of 1Hz as well as the source are correctly identified by the algorithm in all cases. The negative log-likelihoods for all other buses are shown in gray. The amplitude of the forcing is $\gamma=6$, and the time-series correspond to measurements at 50Hz over 400s. The inertia and damping parameters at the generators are heterogeneous and given by $m_i=2.5s^2$, $d_i=1s$ for i=1,2,4,6,7, $m_3=4s^2$, $m_5=1.5s^2$, $d_3=1.6s$, $d_5=1.2s$.

VI. IEEE-57 BUS TEST CASE

The IEEE-57 bus test case [27] we consider here is composed of 7 generators following the dynamics of Eq. (1) and the remaining 50 buses satisfy the algebraic equations given in Eq. (2). Its topology is shown in Fig. 6. Detecting and identifying forced oscillations in this grid appears to be much more challenging than the previous toy model example. Indeed, all the generators are closely clustered, while many loads are far from them in terms of geodesic distance. Also, with measurements from generators only, there are seven times more unobserved buses than accessible ones. One therefore expects the identification to be more complicated, in particular for loads that are far from the generators, as the effective forcing term in the Kron reduced grid might be very much similar or sometimes even identical. For example, the effective forcing Γ_l when the source is located at the blue or green buses are essentially the same, which means that they should be indistinguishable by any algorithm. In the following, we show that the method is able to correctly identify forced oscillations, up to possible degeneracy, where the algorithm will point out to multiple potential locations of the forcing. In all tests, we assume that we learn the parameters by observing the system without forcing during 15min with measurements sampled at 50Hz, and then perform the second step with the forcing using measurement time-series of length 400s also sampled at 50Hz, which is in the typical range for modern PMUs [28], [29]. We stress again that the measurements are only available at generator buses. In the following, we consider a forcing frequency of 1Hz, which is comparable to those observed on actual power grids [4], The inertia and damping parameters are taken as heterogeneous and given in the caption of Fig. 7.

Let us first treat the situation of a forcing applied at generator bus, shown in the left panel of Fig. 7. A forcing of 1Hz is applied at the orange generator in Fig. 6 and unambiguously identified by the maximum of the negative log-likelihood (see left panel Fig. 7).

Next, we consider the more challenging scenario where the forcing is applied at a load/inverter-based resource bus. In

particular, we apply the forcing at the pink bus in Fig. 6. The outcome of the algorithm is shown in the middle panel of Fig. 7 where the method is able to precisely identify the source of forced oscillations, even when the source is far from the generator buses.

Finally, we illustrate the degeneracy discussed previously, where nodes highlighted in green in Fig. 6 is the source of the forcing. As expected, the negative log-likelihoods that we obtain for the blue and the green buses are the same (superimposed green dot and blue curve at 1Hz), as shown in the right panel of Fig. 7. Therefore, up to some degeneracy in the system, our method is able to correctly locate the source of forced oscillations both at unreduced and reduced buses.

VII. COMPARISON WITH EXISTING METHODS

Using the IEEE-57 bus test case, we compare the performance of our maximum likelihood approach (ML) to two recent source localization algorithms: 1) a dissipating energy flow (EF) method [16], [30]; 2) a fully data-based algorithm (SP) that leverages the decomposition of the time-series matrix into the sum of a sparse and a low-rank matrix [31]. While ML can identify sources both at generators and loads, both EF and SP can recover sources solely at measured buses, i.e. at generators. We consider two different amplitudes of the forcing. We start with a case that is a priori simpler to identify. We take the amplitude of the forcing to be significantly larger than the ambient noise, i.e. $\gamma = 10$. Here, when the forcing is applied at generators 1 and 8 (see Tab. I), all three methods successfully recover the source. We then apply the forcing to load buses 4 and 55. EF and SP can only output generator buses by design. When the forcing is at bus 4, EF identifies generator 3 as source. It is worth noting that the latter is directly connected to the actual source. In this case, SP identifies generator 8, which is not directly connected to the actual source. When the forcing is applied at bus 55, EF and SP find respectively generator 9 and 8 as the source while the closest generator bus to the source is bus 9. ML correctly identifies the source of the forcing in both scenarios.

Source	ML	EF	SP
1	1	1	1
8	8	8	8
4	4	3	8
55	55	9	8

TABLE I: Comparison of three forced oscillation identification methods. The maximum likelihood (ML) approach introduced here, a dissipation energy flow (EF) method [16], [30], a fully data-based (SP) method [31]. We stress that forcing applied at load buses are outside the range of applicability EF and SP were designed for. The forcing parameters are $\gamma=10$, $f=1\mathrm{Hz}$.

Source	ML	EF	SP
1	1	1,3	8
8	8	12	8
4	4	8	8
55	55	9	8

TABLE II: Comparison of three forced oscillation identification methods. The maximum likelihood (ML) approach introduced here, an energy dissipation flow (EF) method [16], [30], a fully data-based (SP) method [31]. We stress that forcing applied at load buses are outside the range of applicability EF and SP were designed for. The forcing parameters are $\gamma=1$, $f=1\mathrm{Hz}$.

Next, we turn to more challenging scenarios where the amplitude of the forcing is reduced to $\gamma=1$ (see Tab. II). Compared to Tab. I, one remarks that when the forcing is at the generators, EF and SP identify either the correct source or a generator not the vicinity of it. ML still correctly uncovers the malfunctioning generator. When moving to the forcing applied at the load buses, the conclusions are similar to those for Tab. I .

VIII. WECC 179-BUS SYSTEM

Finally, we test our localization method on realistic datasets. We consider the simulated forced oscillation test cases provided in Ref. [32]. The PMU measurements were generated using a more detailed grid model than the one given in Eqs. (1)-(2). The grid is the WECC 179-bus system base case model and is shown in Fig. 8. Because the library [32] does only provide PMU time-series measurements during oscillations events and not during normal operating conditions, we do not perform step 1 (IV-A) of our method. Instead, we use the parameters given in [32] which are $d_i = 4s \ \forall i \in \mathcal{G}$. We set the inertia parameters as being proportional to the active power of the generators and scale all the inertia parameters such that $\max_i m_i = 20s^2$. As our method neglects ohmic losses on the transmission lines, we built the Laplacian matrix of the grid from the positive line susceptance parameters, which yields a disconnected grid. In the three cases considered here, namely the F_2, F_3 and 6F_1, we keep only the connected part of the grid where the event is happening i.e. generator buses 30, 35, 65, 70, 77, 79, and load buses 31, 32, 33, 34, 66, 67, 68, 69, 71, 72, 73, 74, 75, 76, 78, 80, 82, 87, 91, 95 in Fig. 8. In terms of PMU measurements, this means

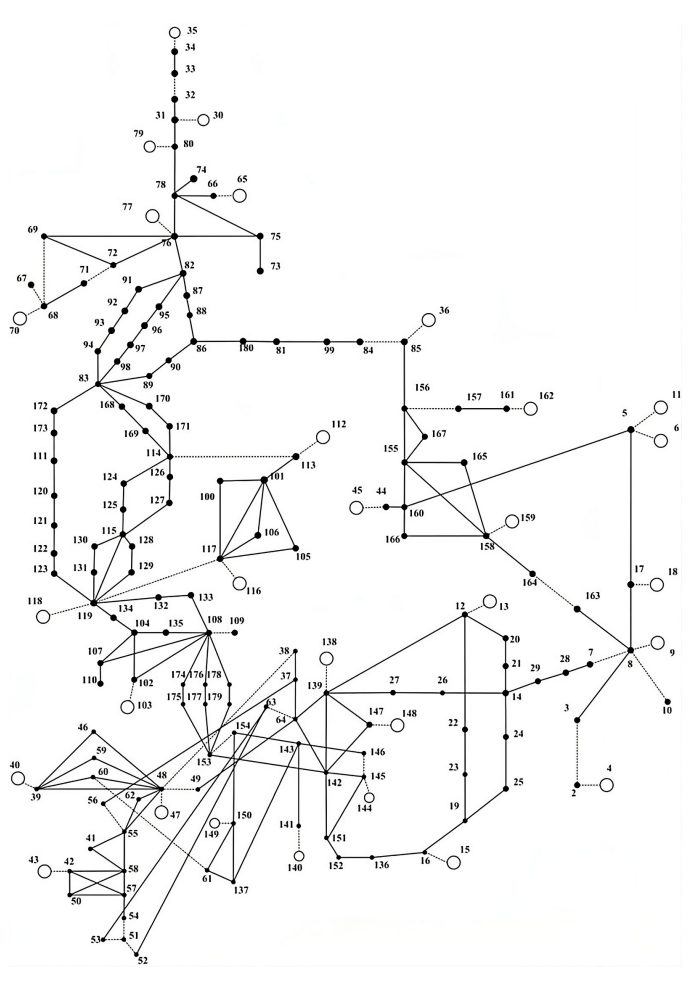


Fig. 8: Topology of the WECC 179-bus system from the library [32]. Empty circles represent generators while filled circles correspond to substations and load buses.

that the input of our algorithm is 6 angle and 6 frequency timeseries whose length is 40s. Below, we apply step 2 (IV-B) of our method on three different test cases from [32].

A. Test case F_2

The first case we investigate is the F_2 from the library provided in Ref. [32]. For this simulated event, a forced sinusoidal signal is injected into the excitation system at generator 79 (top of Fig. 8) with a frequency f = 0.86Hz, which is close to a natural mode of the grid. In Fig. 9 we show the outcome of the method, i.e. the values of the negative log-likelihood for all possible location and frequency of the forced oscillation. The blue dots correspond to the generator 79 which is identified as the generator bus with the largest value around the actual forcing frequency $f \cong 0.86 \mathrm{Hz}$. The green and orange symbols which have the same negative likelihood correspond to load buses 78 and 74. Our method doesn't identify the actual source correctly, even though it is among the largest negative likelihood values. The two load buses that are found by the method are close to the actual source.

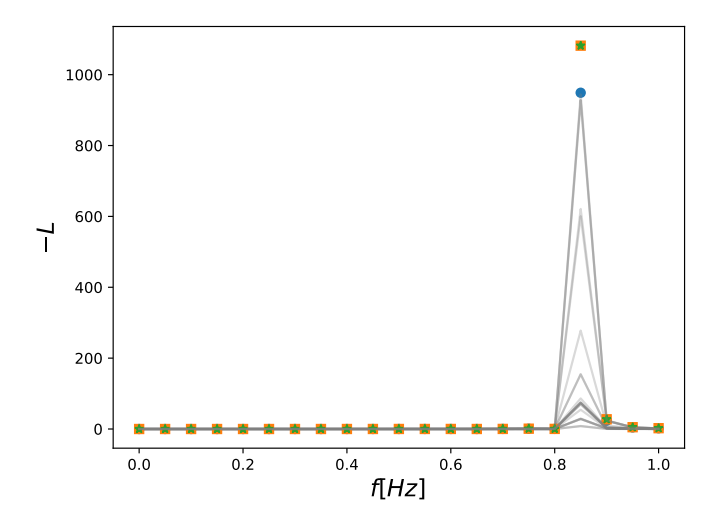


Fig. 9: Detection and localization of forced oscillations for the test case F_2 from the library [32]. The forcing of $f=0.86 \mathrm{Hz}$ is applied at the generator bus 79. The blue dots correspond to the negative log-likelihood for generator 79; The green and orange symbols which have the same negative likelihood correspond respectively to bus 78 and bus 74; the grey lines correspond to all the other buses.

B. Test case F 3

Then, we move to the case F_3 where a forced sinusoidal signal is injected into the excitation system at generator 77 (top of Fig. 8) with a frequency $f=0.37 \mathrm{Hz}$. In Fig. 10, one observes that our method fails to identify the generator 77 as the sources of the forced oscillation. Instead, the generator 65 (orange squares) is found to be the source, with bus 66 (green stars) having a similar value for the negative log-likelihood. Both of them are close to the actual source whose log-likelihood is given by the blue dots.

C. Test case F_6_1

Finally, we consider the case F_6_1 where the forcing is a rectangle wave with fundamental frequency $f=0.1 {\rm Hz}$ injected into the excitation system of generator 79. The results are shown in Fig. 11 where one observes that the identified source at $f=0.1 {\rm Hz}$ is generator 30 (blue dots), which is close to the actual source whose log-likelihood is given by the orange triangles. The largest negative likelihood is found at $f=0.7 {\rm Hz}$ where both bus 74 (green squares) and bus 78 (red stars) have similar values. These buses are also rather close to the actual source. Therefore, the method still provides important information about the source of forced oscillations in this case.

IX. CONCLUSION

Due to the aging of the existing grid assets and the ongoing energy transition that considerably enhances the fluctuations and increases the number of inverter-based resources connected to the grid, forced oscillations are expected to become more prevalent, while making the problem of locating them

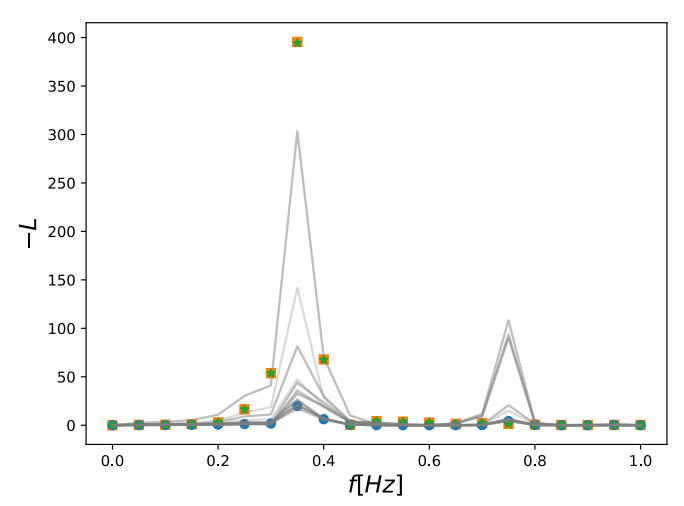


Fig. 10: Detection and localization of forced oscillations for the test case F_3 from the library [32]. The forcing of $f=0.37 \mathrm{Hz}$ is applied at the generator bus 77 (blue dots). The orange squares correspond to the negative log-likelihood for generator 65; the green stars for bus 66; the grey lines correspond to all the other buses.

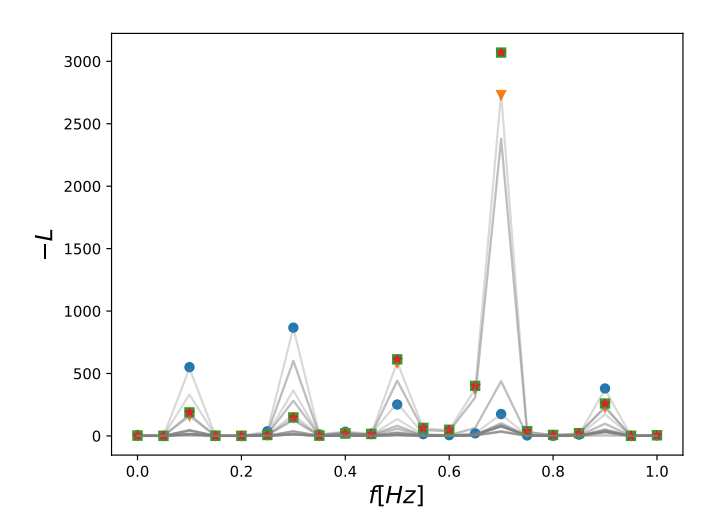


Fig. 11: Detection and localization of forced oscillations for the test case $6F_1$ from the library [32]. The forcing of f=0.1Hz is a rectangle wave and is applied at the generator bus 79 given by the orange triangles. The blue dots correspond to the negative log-likelihood for generator 30, which is close to the actual source in Fig. 8; green squares and red stars correspond respectively to bus 74 and 78 which are also close to the actual source; the grey lines correspond to all the other buses.

much harder. Here, we proposed a data driven algorithm that uses prior knowledge about the grid to locate the source and identify the frequency of forced oscillations in transmission power grids. We considered a system composed of traditional generators with second-order swing dynamics, and loads/inverter-based resources that satisfy algebraic equations and thus do not have intrinsic dynamics. By means of a Kron reduction, we focused on time-series measurements observed at generator buses which are used, together with the Kron-reduced Laplacian matrix, first to learn the inertia and damping parameters when there is no forcing, and second to define a log-likelihood function that we then optimize. The method is able to identify correctly forced oscillations when the source is located at generator and load/inverterbased resource buses. Our method correctly pinpoints the source or a set of equivalent sources, even when the number of observed generator buses is much smaller than the total number of buses in the original grid. Importantly, it is able to identify the source of forced oscillations even when the later is not directly measured. Eventually, we tested the algorithm on realistic PMU measurements simulated using grid and generator models that are more detailed than the ones assumed by our method. In this brief exploration, we found that our localization algorithm can provide useful information about the actual source of the forced oscillation. In the three cases tested here, it identified generators or buses close to the actual source, using a scarce amount of data. This is promising for the next development of the method to account for more detailed grid dynamics.

Further work should consider forced oscillation source localization under the assumption of a limited prior knowledge on the Kron-reduced Laplacian matrix, and under the case of incomplete observation of generators in the grid. One may include as well heterogeneous standard deviations of the noise [33] in the optimization and account for time-correlation [34]. Eventually, one should extend the method to account for natural oscillations and oscillations originating from spurious signals injected into the generator using more detailed dynamics.

APPENDIX

A. Details about likelihood functions

Here, we give details about the steps to go from the likelihood function Eq. (14) to the equivalent form Eq. (19). In Eq. (14), one has

$$\frac{1}{N} \sum_{i=0}^{N-1} \mathbf{v}_{t_i}^{\top} \mathbf{\Sigma}_{gl}^{-1} \mathbf{v}_{t_i} = [\mathbf{\Delta}_{t_i}]_{2}^{\top} \mathbf{M}^{\top} \mathbf{\Sigma}_{gl}^{-1} \mathbf{M} [\mathbf{\Delta}_{t_i}]_{2}
+ [\mathbf{A} \mathbf{X}_{t_i}]_{2}^{\top} \mathbf{M}^{\top} \mathbf{\Sigma}_{gl}^{-1} \mathbf{M} [\mathbf{A} \mathbf{X}_{t_i}]_{2}
- [\mathbf{A} \mathbf{X}_{t_i}]_{2}^{\top} \mathbf{M}^{\top} \mathbf{\Sigma}_{gl}^{-1} \mathbf{M} [\mathbf{\Delta}_{t_i}]_{2}
- [\mathbf{\Delta}_{t_i}]_{2}^{\top} \mathbf{M}^{\top} \mathbf{\Sigma}_{gl}^{-1} \mathbf{M} [\mathbf{A} \mathbf{X}_{t_i}]_{2}
- [\mathbf{\Delta}_{t_i} - \mathbf{A} \mathbf{X}_{t_i}]_{2}^{\top} \mathbf{M}^{\top} \mathbf{\Sigma}_{gl}^{-1} \mathbf{u}(k)
- \mathbf{u}(k)^{\top} \mathbf{\Sigma}_{gl}^{-1} \mathbf{M} [\mathbf{\Delta}_{t_i} - \mathbf{A} \mathbf{X}_{t_i}]_{2} ,$$
(28)

where in the latter equation, only the last two terms depend on γ , l, k, ϕ . The other terms can therefore be dropped

to define a new likelihood function that will have the same extrema as the original one. Then, to obtain Eq. (19), one performs the explicit optimization over the phase ϕ , noticing that only a single term actually depends on the ϕ , which is $-\frac{2\gamma}{\sqrt{N}} \left| \mathbf{\Gamma}_l^{\mathsf{T}} \mathbf{\Sigma}_{\mathbf{gl}}^{-1} \mathbf{M}(\tilde{\mathbf{\Delta}} - \mathbf{A}\tilde{\mathbf{X}}) \right|$. Rewriting the modulus using traces and rearranging terms yields the expression in Eq. (19).

REFERENCES

- "NERC report: Reliability Guideline Forced Oscillation Monitoring & Mitigation," accessed: 2024-02-5.
- [2] S. A. N. Sarmadi and V. Venkatasubramanian, "Inter-area resonance in power systems from forced oscillations," *IEEE Trans. Power Syst.*, vol. 31, no. 1, pp. 378–386, 2015.
- [3] "NERC report: Eastern Interconnection Oscillation Disturbance January 11, 2019 Forced Oscillation Event," accessed: 2023-09-29.
- [4] M. Ghorbaniparvar, "Survey of forced oscillations in power systems," J. Mod. Syst. Clean Energy, vol. 5, no. 5, pp. 671–682, 2017.
- [5] P. W. Sauer, M. A. Pai, and J. H. Chow, Power System Dynamics and Stability: With Synchrophasor Measurement and Power System Toolbox. John Wiley & Sons, 2017.
- [6] A. Y. Lokhov, M. Vuffray, D. Shemetov, D. Deka, and M. Chertkov, "Online learning of power transmission dynamics," in 2018 Power Systems Computation Conference (PSCC), June 2018, pp. 1–7.
- [7] A. Y. Lokhov, D. Deka, M. Vuffray, and M. Chertkov, "Uncovering power transmission dynamic model from incomplete pmu observations," in 2018 IEEE Conference on Decision and Control (CDC). IEEE, 2018, pp. 4008–4013.
- [8] L. R. Gorjão, M. Anvari, H. Kantz, C. Beck, D. Witthaut, M. Timme, and B. Schäfer, "Data-driven model of the power-grid frequency dynamics," *IEEE access*, vol. 8, pp. 43 082–43 097, 2020.
- [9] C. Hannon, D. Deka, D. Jin, M. Vuffray, and A. Y. Lokhov, "Real-time anomaly detection and classification in streaming pmu data," in 2021 IEEE Madrid PowerTech. IEEE, 2021, pp. 1–6.
- [10] B. C. Lesieutre, Y. Abdennadher, and S. Roy, "Model-enhanced localization of forced oscillation using pmu data," in 2022 58th Annual Allerton Conference on Communication, Control, and Computing (Allerton). IEEE, 2022, pp. 1–8.
- [11] I. R. Cabrera, B. Wang, and K. Sun, "A method to locate the source of forced oscillations based on linearized model and system measurements," *Proc. of the IEEE PESGM*, 2017.
- [12] R. Delabays, L. Pagnier, and M. Tyloo, "Locating line and node disturbances in networks of diffusively coupled dynamical agents," *New J. Phys.*, vol. 23, p. 043037, 2021.
- [13] T. R. Nudell and A. Chakrabortty, "A graph-theoretic algorithm for disturbance localization in large power grids using residue estimation," in 2013 Amercian Control Conference (ACC). IEEE, 2013, pp. 3467– 3472
- [14] A. Semerow, S. Horn, B. Schwarz, and M. Luther, "Disturbance localization in power systems using wide area measurement systems," in *IEEE International Conference on Power System Technology (POWERCON)*. IEEE, 2016.
- [15] L. Chen, Y. Min, and W. Hu, "An energy-based method for location of power system oscillation source," *IEEE Trans. Power Syst.*, vol. 28, no. 2, pp. 828–836, 2013.
- [16] S. Maslennikov, B. Wang, and E. Litvinov, "Dissipating energy flow method for locating the source of sustained oscillations," *Int. J. Elec. Power & Energy Syst.*, vol. 88, pp. 55–62, 2017.
- [17] S. Chevalier, P. Vorobev, and K. Turitsyn, "Using effective generator impedance for forced oscillation source location," *IEEE Trans. Power Syst.*, vol. 33, no. 6, pp. 6264–6277, 2018.
- [18] —, "A bayesian approach to forced oscillation source location given uncertain generator parameters," *IEEE Trans. Power Syst.*, vol. 34, no. 2, pp. 1641–1649, 2019.
- [19] T. Huang, N. M. Freris, P. R. Kumar, and L. Xie, "Localization of forced oscillations in the power grid under resonance conditions," *Proc. of the IEEE CISS*, 2018.
- [20] Z. Chen and J.-C. Maun, "Artifical neural network approach to single-ended fault locator for transmission lines," *IEEE Trans. Power Syst.*, vol. 15, no. 1, pp. 370–375, 2000.
- [21] G. Cardoso, J. G. Rolim, and H. H. Zürn, "Application of neural-network modules to electric power system fault section estimation," *IEEE Trans. Power Deliver.*, vol. 19, no. 3, pp. 1034–1041, 2004.

- [22] H.-W. Lee, J. Zhang, and E. Modiano, "Data-driven localization and estimation of disturbance in the interconnected power system," in *IEEE International Conference on Communications, Control, and Computing Techologies for Smart Grids (SmartGridComm)*. IEEE, 2018.
- [23] R. Delabays, A. Y. Lokhov, M. Tyloo, and M. Vuffray, "Locating the source of forced oscillations in transmission power grids," *PRX Energy*, vol. 2, no. 2, p. 023009, 2023.
- [24] G. Kron, "Tensor analysis of networks," New York, vol. 146, 1939.
- [25] F. Dörfler and F. Bullo, "Kron reduction of graphs with applications to electrical networks," *IEEE Transactions on Circuits and Systems I: Regular Papers*, vol. 60, no. 1, pp. 150–163, 2012.
- [26] P. Kundur, N. J. Balu, and M. G. Lauby, Power system stability and control. McGraw-hill New York, 1994, vol. 7.
- [27] "IEEE 57-bus test case," http://www.ee.washington.edu/research/pstca/ \pf57/pg_tca57bus.htm, accessed: 2024-03-08.
- [28] A. Silverstein, J. Follum et al., "High-resolution, time-synchronized grid monitoring devices," NA Synchrophasor Initiative, Tech. Rep. NAPSI-2020-TR-004, 2020.
- [29] S. Maslennikov and B. Wang, "Creation of simulated test cases for the oscillation source location contest," in 2022 IEEE Power & Energy Society General Meeting (PESGM). IEEE, 2022, pp. 1–1.
- [30] L. Ying, S. Chen, and L. Feng, "An energy-based methodology for locating the source of forced oscillations in power systems," in 2012 IEEE International Conference on Power System Technology (POWERCON). IEEE, 2012, pp. 1–6.
- [31] T. Huang, N. M. Freris, P. Kumar, and L. Xie, "A synchrophasor data-driven method for forced oscillation localization under resonance conditions," *IEEE Transactions on Power Systems*, vol. 35, no. 5, pp. 3927–3939, 2020.
- [32] S. Maslennikov, B. Wang, Q. Zhang, E. Litvinov et al., "A test cases library for methods locating the sources of sustained oscillations," in 2016 IEEE Power and Energy Society General Meeting (PESGM). IEEE, 2016, pp. 1–5.
- [33] J. Hindes, I. B. Schwartz, and M. Tyloo, "Stability of kuramoto networks subject to large and small fluctuations from heterogeneous and spatially correlated noise," *Chaos: An Interdisciplinary Journal of Nonlinear Science*, vol. 33, no. 11, 2023.
- [34] M. Tyloo and P. Jacquod, "Primary control effort under fluctuating power generation in realistic high-voltage power networks," *IEEE Control* Systems Letters, vol. 5, no. 3, pp. 929–934, 2020.